Role of anodically electrogenerated hydroxyl radicals on minimizing mineral cathodic electroprecipitation in the presence of hard water

Faidzul Hakim Adnan, Steve Pontvianne, Marie-Noëlle Pons, Emmanuel Mousset

Electrochemistry Communications 150 (2023) 107493

Contents lists available at ScienceDirect

Electrochemistry Communications

journal homepage: www.elsevier.com/locate/elecom

Full Communication

Role of anodically electrogenerated hydroxyl radicals in minimizing mineral cathodic electroprecipitation in the presence of hard water

Faidzul Hakim Adnan [a,b], Steve Pontvianne [a], Marie-Noëlle Pons [a,c], Emmanuel Mousset [a,*]

[a] Université de Lorraine, CNRS, LRGP, F-54000 Nancy, France
[b] Sustainable Process Engineering Centre (SPEC), Department of Chemical Engineering, Faculty of Engineering, Universiti Malaya, 50603 Kuala Lumpur, Malaysia
[c] LTSER-LRGP, CNRS, Université de Lorraine, F-54000 Nancy, France

ARTICLE INFO

Keywords:
Calcium carbonate
Electrooxidation
Electroprecipitation
Microfluidic reactor
Modelling
Wastewater treatment

ABSTRACT

Electrochemical systems are attracting increasing interest in environmental protection as relatively sustainable processes, particularly in wastewater treatment and reuse. However, cathode scaling in electrochemical processes for wastewater treatment is a major issue that is often overlooked. It is proposed for the first time to investigate the anodic contribution towards $CaCO_3$ electroprecipitation phenomena under the advanced electrooxidation conditions applied to remove organic biorecalcitrant pollutants. The contribution of the reaction of the hydroxyl radical ($^{\bullet}OH$) with carbonates, which reduces cathodic scaling at a micrometric interelectrode distance (500 μm) and at a high current density (16 mA cm^{-2}), is described in detail. In addition, the anti-scaling effect of local anodic acidification should be considered. A new kinetic model of electroprecipitation fits the experimental curves well (root mean square error (RMSE) < 0.19 for Ca^{2+}) and confirms this anodic role, combined with the gas hindrance and scale detachment induced by gas bubble electrogeneration at sufficiently high current intensities.

1. Introduction

As a result of more stringent regulations on the release of wastewater into aquatic media which have been designed to preserve the natural environment and to promote water reuse, the conventional biological and physicochemical treatments used in wastewater treatment plants (WWTPs) may soon no longer be sufficient [1–3]. Thus, a variety of complementary treatments has been proposed in the literature, and some have been applied at an industrial scale [4–7]. The majority of these processes operate using chemical oxidation with strong oxidants to eliminate pollutants [8–11]. These processes include classical oxidation processes such as chlorination, ozonation and ultraviolet irradiation, and, more recently, advanced oxidation processes (AOPs) designed to degrade organic contaminants. However, this increased efficiency comes with a high price tag: the requirement to use chemical reagents (e.g., H_2O_2, Cl_2, O_3, acid/base, Fe^{2+}, etc.) [12,13], which goes against the environmentally friendly approach to wastewater treatment. One category of AOPs is electrochemical advanced oxidation processes (EAOPs) [3,5,12,14–18], in which potent, quasi non-selective oxidizing agents such as hydroxyl radicals ($^{\bullet}OH$) and other mediated oxidants (e.g., hydrogen peroxide (H_2O_2), $HClO/ClO^-$, Cl_2, O_3, etc.) are electrogenerated in situ [18–20].

In the last decade, the introduction of submillimetric reactors within EAOPs has broadened the perspective of water treatment using electrochemical techniques [21–28]. A micrometric interelectrode distance could lift the mass transport limitation often encountered in macrometric electrochemical reactors [21,29]. Redox activities on each electrode could also contribute and may result in changes to the overall electrochemical/chemical reactions in the system [30]. This approach also makes it possible to operate with low-conductivity solutions, while minimizing the energy requirement [31–33].

However, electrolytic systems remain prone to electrode passivation, even under microfluidic conditions [30,34]. Depending on the potential applied to the cathode, the reduction of dissolved oxygen (O_2) (Eq. (1)) and/or water (Eq. (2)) occurs [35,36]:

$$O_2 + 2H_2O + 4e^- \rightarrow 4OH^- \quad (1)$$

$$2H_2O + 2e^- \rightarrow H_2 + 2OH^- \quad (2)$$

These reactions lead to a gradient in the hydroxyl ion (OH^-) concentration near the cathode compared to that in bulk solution. A high local pH [30,34,37] during electrolysis could easily convert CO_3^{2-} into its

* Corresponding author.
E-mail address: emmanuel.mousset@cnrs.fr (E. Mousset).

https://doi.org/10.1016/j.elecom.2023.107493
Received 20 October 2022; Received in revised form 18 April 2023; Accepted 20 April 2023
Available online 25 April 2023

predominant form, according to the acid–base constants given in Eqs. (3)-(4) [38,39]:

$$K_{A1} = \frac{[H^+][HCO_3^-]}{[H_2CO_3]}, pK_{A1} = 6.3 \quad (3)$$

$$K_{A2} = \frac{[H^+][CO_3^{2-}]}{[HCO_3^-]}, pK_{A2} = 10.4 \quad (4)$$

Thus, depending on the concentration of magnesium (Mg^{2+}) and calcium (Ca^{2+}) ions in the effluent to be treated, Mg- and Ca-based passivating layers could be formed on the cathode surface, as shown in Eqs. (5)-(7):

$$Mg^{2+} + 2OH^- \rightarrow Mg(OH)_2 \quad (5)$$

$$OH^- + HCO_3^- \rightarrow H_2O + CO_3^{2-} \quad (6)$$

$$Ca^{2+} + CO_3^{2-} \rightarrow CaCO_3 \quad (7)$$

Such passivation layers can strongly impact the durability of EAOPs under continuous operation if regular and costly maintenance is not foreseen. Mechanical clean-in-place (CIP) techniques have demonstrated high descaling efficiency with smooth materials [40]. However, such methods are likely to be less useful for porous materials, bearing in mind that the electro-precipitates are located within the internal pores [41]. Most EAOPs require the use of porous material electrodes, particularly to implement flow-through design to increase mass transport [22,27,31,42]. Periodic polarity reversal is another successful descaling technique, which has been applied at industrial scale to prolong the electrodialysis process [43–46]. However, this technique may not be suitable for most EAOPs. Efficient descaling using this technique could only be obtained using a high applied current (I_{app}) [43,44,47,48], which translates into an elevated overall operational cost. Also, only stable electrodes, such as several mixed metal oxides (MMO) (e.g. IrO_2–RuO_2/Ti, IrO_2–RuO_2–SnO_2/Ti), Pt-coated Ti or boron-doped diamond (BDD), which are capable of resisting high current polarization in both cathode and anode configurations. Other common electrode materials (e.g., most steels and less noble metals) become corroded via anodic polarization at high I_{app}, releasing ions into the solution. Carbonaceous materials can even be burnt when they are used as anodes under medium and high current densities [49]. Thus, reducing the frequency of polarity reversal or even proposing an alternative to avoid this technique by a self-cleaning mechanism would challenge the current practice and enlarge the application field of applied electrochemistry, including EAOPs.

Surprisingly, the role of $^{\bullet}OH$ in mineral scale formation has never been studied and is thus the goal of this study. Moreover, the involvement of anodic activity is typically stronger under microfluidic conditions and may play a role in the mechanism of electroprecipitation on the cathode and on pollutant degradation via $^{\bullet}OH$ generated at the anode or mediated oxidants in the bulk. HCO_3^-/CO_3^{2-} is a $^{\bullet}OH$ scavenger via the formation of carbonate radicals [50,51], which could reduce the carbonate concentration available near the cathode, possibly resulting in less calcareous scaling. This hypothesis is studied for the first time in this paper using a systematic investigation using synthetic wastewater while progressively increasing the applied current density to assess the influence of anodic $^{\bullet}OH$ on cathodic mineral scaling.

2. Materials and methods

2.1. Chemicals

Information about the chemicals used in this study is given in the Supplementary Information (Text S1).

2.2. Preparation of effluent

Experiments were performed using a synthetic effluent containing 3.75 mmol L^{-1} (150 mg of L^{-1}) Ca^{2+}, 0.21 mmol L^{-1} (5 mg of L^{-1}) Mg^{2+} and 5 mmol L^{-1} (60 mg of C L^{-1}) bicarbonates by dissolving 1.2887 g of $CaSO_4{\cdot}2H_2O$, 0.1014 g of $MgSO_4{\cdot}7H_2O$ and 0.8400 g of $NaHCO_3$ in 2 L of ultrapure water (18.2 MΩ cm) provided by a PureLab ELGA water purification dispenser (Veolia Water, Antony, France). No additional supporting electrolyte was used. The initial pH was adjusted to 7.6 by adding 650 μL of 1 mol L^{-1} sulfuric acid. The eventual electrical conductivity of the synthetic effluent was approximately 1000 μS cm^{-1}, with the ionic strength estimated to be 0.02 mol L^{-1}. These properties were selected to emulate the characteristics of municipal wastewater plant effluent [30,34].

2.3. Electrochemical setup

The electrochemical setup consisted of a vertical parallel-plate filter press reactor, composed of a stainless steel cathode and a BDD anode separated by a spacer of 500 μm thick. The setup is described elsewhere [29,30,34,41] and more details are given in the Supplementary Text S3.

2.4. Analytical methods

Details of the analytical methods used in this study are given in the Supplementary Text S2.

2.5. Development of the electroprecipitation model

Our model of electroprecipitation kinetics is based on recent studies in which the electroprecipitations occurring within submillimetric to millimetric interelectrode distances were modeled [30,34]. Continuous reduction of dissolved O_2 (Eq. (1)) and H_2O (Eq. (2)) to OH^- could be modeled via a modified Faraday's law as shown in Eqs. (8)-(9):

$$r_{OH^-} = +\frac{d[OH^-]}{dt} = \frac{\nu_{O_2} j_{app}}{n_{O_2} F} CE_{O_2} + \alpha \frac{j_{app}}{F} \quad (8)$$

$$\alpha = \nu_{H_2O} \frac{CE_{H_2O}}{n_{H_2O}} - \nu_{H_2} \frac{CE_{H_2}}{n_{H_2}} \quad (9)$$

where r_{OH^-} is the heterogeneous production rate of OH^- (mol m^{-2} min^{-1}) (the concentration is expressed in mol m^{-2} due to negligible thickness of the reaction zone with respect to the electrode surface [30]); α is the gas hindrance factor related to H_2 bubble production on the cathode originating from the H_2O reduction reaction shown in Eq. (2) [30]; j_{app} is the applied current density (A m^{-2}); F is the Faraday constant (96,485 C mol^{-1}); n_{O_2} (=4) and n_{H_2O} (=2) are the numbers of electrons participating in Eq. (1) and Eq. (2), respectively [30,34]; n_{H_2} (=2) reacted to produce H_2 with respect to the stoichiometry of OH^- production from Eq. (2); ν_{O_2} (=4) and ν_{H_2O} (=2) are the stoichiometric coefficients of OH^- produced by Eq. (1) and Eq. (2), respectively; ν_{H_2} (=1) is the stoichiometry of H_2 production with respect to that of OH^- in Eq. (2); CE_{O_2} and CE_{H_2O} are the current efficiencies attributed to the Faradaic reactions in Eq. (1) and Eq. (2); and CE_{H_2} is the proportion of Faradaic current spent due to the concomitant H_2 evolution in Eq. (2). CE_{O_2} and CE_{H_2O} were determined experimentally at different applied currents using the Ti(IV)–H_2O_2 complexation method described elsewhere [30,52]. Because CE_{H_2O} and CE_{H_2} appear in the same half equation of Eq. (2) whereby the reduction of H_2O and the evolution of H_2 take place on the same cathodic surface, it has been hypothesized that the current efficiency CE_{H_2} equals CE_{H_2O} [30]. Thus, α (Eq. (9)) can also be deduced. The current efficiencies and the value of α as a function of the applied current are summarized in Table S1. Detailed explanations and calculations are given in the Supplementary Text S4.

The rate of $CaCO_3$ electroprecipitation (r_{CaCO_3}) was modeled using

the kinetic laws given in Eqs. (10)-(11):

$$r_{Ca^{2+}} = -r_{CaCO_3} = -\left(k_{CaCO_3} - k_{det,CaCO_3}\right)\left[Ca^{2+}\right]\left[CO_3^{2-}\right]_{int} \quad (10)$$

$$\left[CO_3^{2-}\right]_{int} = \frac{K_{A2} \times [TIC]}{\frac{K_w}{[OH^-]} + K_{A2}} - k_{\bullet OH}.[TIC].t \quad (11)$$

where $r_{Ca^{2+}}$ is the rate of heterogeneous Ca^{2+} precipitation (mol m^{-2} min^{-1}); k_{CaCO_3} is the second-order rate constant of heterogeneous electroprecipitation of $CaCO_3$ (3.6×10^{-3} m^4 mol^{-1} min^{-1} [30,34]; $k_{det,CaCO_3}$ (m^4 mol^{-1} min^{-1}) is the $CaCO_3$ detachment rate constant due to concomitant evolving gas, which is dependent on the applied current; $\left[Ca^{2+}\right]$ is the molar concentration of Ca^{2+} (mol m^{-3}); K_{A2} is the acidity constant of the HCO_3^-/CO_3^{2-} acid–base couple (Eq. (4)) ($pK_{A2} = 10.4$ [38]); and $\left[CO_3^{2-}\right]_{int}$ is the theoretical interfacial concentration of carbonates on the cathode (mol m^{-3}), which is modeled using Eq. (11). Eq. (11) is a function of **(1)** the concentration (mol m^{-3}) of total inorganic carbon ([TIC], defined as $[HCO_3^-] + [CO_3^{2-}]$), ignoring carbonic acid given the range of investigated pH values in the bulk and **(2)** the concentration of OH^- produced via Eqs. (8)-(9). $k_{\bullet OH}$ is newly introduced and represents the pseudo first-order rate constant for conversion of carbonates into carbonate radicals ($CO_3^{\bullet -}$) by the intermediary $^{\bullet}OH$ (min^{-1}) under conditions where the latter is present.

The modeling of Ca^{2+} concentration evolution was performed using Aquasim® software [53]. The root mean square error (RMSE) (Eq. (12)) [54] was used to determine the fit between experimental and modeled points:

$$RMSE = \sqrt{\frac{\sum_{i=1}^{K}\left(y_i - y_i^{'}\right)^2}{K}} \quad (12)$$

where $y_i^{'}$ is the experimental value, y_i is the model value and K is the number of iteration.

3. Results and discussion

3.1. Kinetics of electroprecipitation of $CaCO_3$ at different applied currents

Fig. 1 shows the evolution of the experimental and modeled Ca^{2+} and total inorganic carbon (TIC) concentrations during electrolysis at 40, 200 and 800 mA. Ca^{2+} precipitated at 54.4 ± 1.9%, 49.8 ± 5.6% and 46.9 ± 1.2% at 40, 200 and 800 mA, respectively, while TIC precipitated at 92.4 ± 3.9%, 87.6 ± 1.7% and 84.4 ± 4.8% with increasing I_{app}. A rise in $CaCO_3$ electroprecipitation was noted as I_{app} was increased. The associated changes in bulk pH and ionic conductivity are displayed in Fig. S1 and discussed in the Supplementary Text S5.

Fig. 2 shows the molar ratio of Ca^{2+} concentration with respect to TIC concentration over the course of a 5 h electrolysis as well as the molar ratio of precipitated Ca^{2+} compared to precipitated carbonates. In Fig. 2a, the ratio $[Ca^{2+}]/[TIC]$ was less than one (0.64 to 0.77) because there were more moles of carbonate than of Ca^{2+}, meaning that the concentration of Ca^{2+} was the limiting factor. As the electrolysis time increased, the ratio $[Ca^{2+}]/[TIC]$ increased due to a decrease in both Ca^{2+} and carbonate concentrations, which suggests that the consumption of the latter was quicker than that of the former. This result is supported by the TIC plot in Fig. 1b. The quicker decrease in carbonate compared to Ca^{2+}, whatever the applied current, could be due to their protonation into carbonic acid and then into CO_2, caused by the local acidification at the anode surface through H_2O oxidation. The deduction made from Fig. 1 was replicated in this study (see Fig. 2b). The molar ratio of precipitated $\Delta[Ca^{2+}]$ over $\Delta[TIC]$ at the end of electrolysis was determined to be 0.39 ± 0.02, 0.40 ± 0.04 and 0.35 ± 0.02 for 40, 200 and 800 mA current, respectively. The ratio $\Delta[Ca^{2+}]/\Delta[TIC]$ was the lowest at the highest I_{app} (800 mA). This lower ratio was the outcome of lower precipitation of Ca^{2+} (i.e., higher Ca^{2+} content in the bulk) and could also be due to the reaction of carbonates with other compounds, which is discussed in Sections 3.3 and 3.4.

3.2. Role of measured electrode potentials on $CaCO_3$ electroprecipitation at different applied currents

When an electrochemical cell is polarized at a given I_{app} using a current generator, a specific potential will eventually be applied to both the anode and the cathode. The applied potentials depend on the applied current and on the configuration of the electrochemical reactor [29,30]. Fig. 3 shows the cathode potential (E_C) as a function of the percentage of $CaCO_3$ deposited, together with the anode potential (E_A), cell voltage (ΔU) and ohmic drop ($\sum RI$) at all investigated I_{app} values. In agreement with Fig. 3a, E_C was found to be −1.40, −1.54 and −2.30 V/Ag-AgCl when the current was 40, 200 and 800 mA, respectively. A previous study showed that as E_C falls deeper into the water reduction region [30], E_C moves further away from the standard potential of O_2 reduction into OH^- via four electrons (Eq. (1)), which occurs with minimum parasitic hydrogen gas (H_2) formation [55,56]. The importance of gas evolution on cathode scaling was emphasized in a recent article dealing with the effect of d_{elec} [30]. The increase in d_{elec} decreased E_C and thus increased scale detachment. Similarly, as a higher I_{app} is applied in this study, a lower percentage of cathodic $CaCO_3$ deposition was observed, partly due to the detachment associated with intense H_2 evolution.

Also, as I_{app} increased, the measured E_A and ΔU also increased. E_A was experimentally determined to be 2.19, 2.50 and 2.78 V/Ag-AgCl,

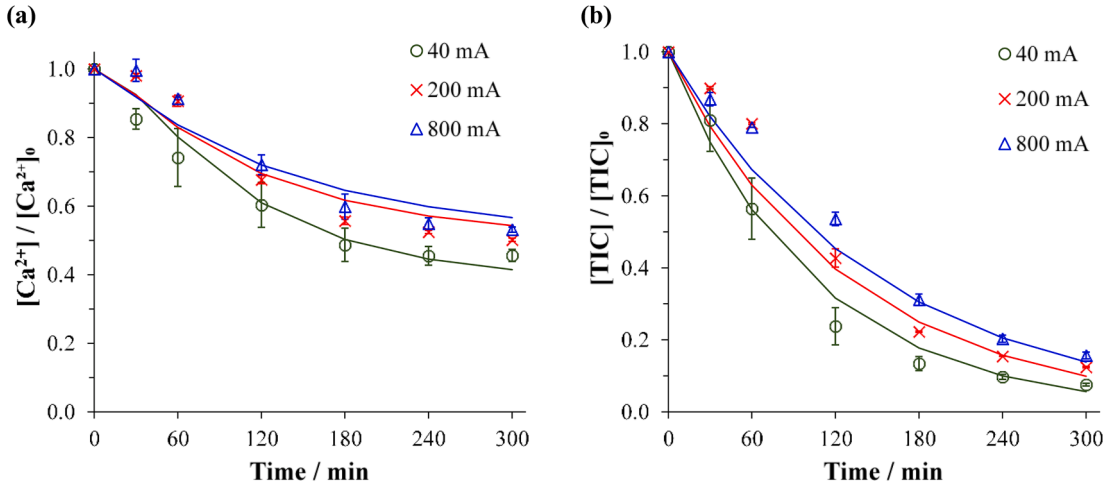

Fig. 1. Experimental and modeled kinetics of the concentration of (a) Ca^{2+} and (b) TIC at 40, 200 and 800 mA.

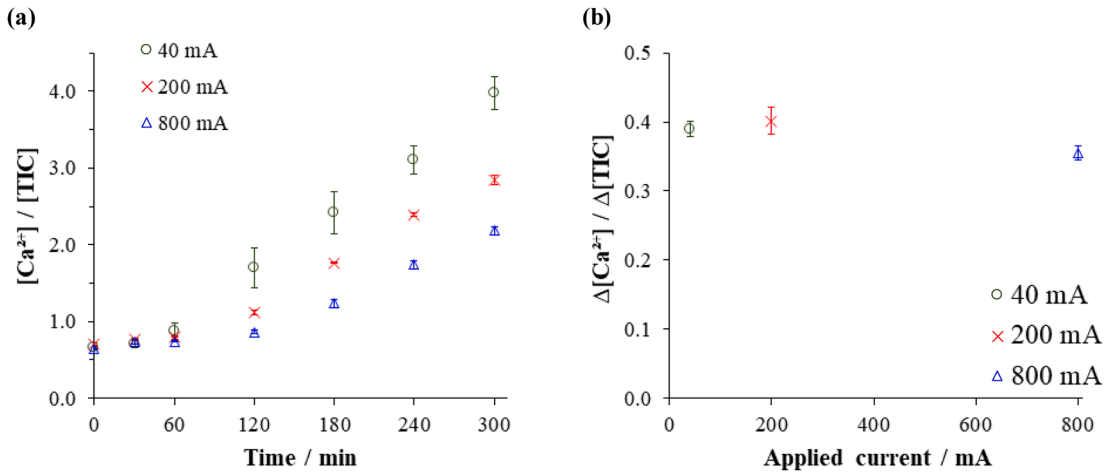

Fig. 2. Molar ratio of (a) Ca^{2+} concentration with respect to that of TIC and (b) precipitated Ca^{2+} with respect to precipitated carbonates.

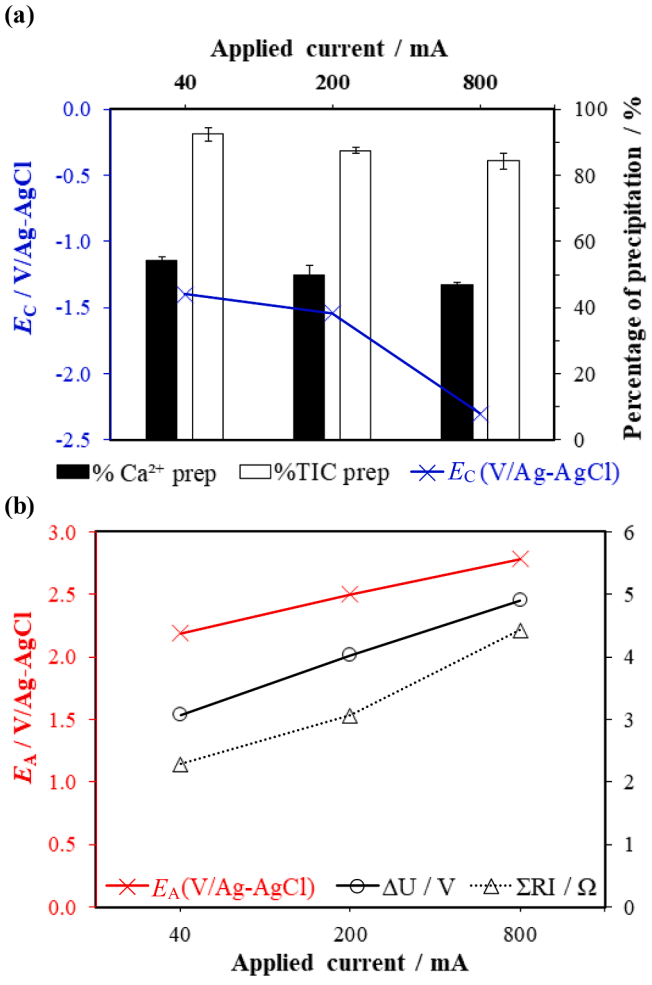

Fig. 3. Relationship between (a) measured E_C with the percentage of electro-precipitation and (b) measured E_A, ΔU and the corresponding $\sum RI$ as a function of applied current.

while ΔU was measured to be 3.07, 4.03 and 4.90 V at currents of 40, 200 and 800 mA, respectively. This increase in cell voltage was expected because a higher I_{app} was applied. As I_{app} increased, overpotentials on both the anode and cathode also increased with respect to the equilibrium potentials [57]. H_2 and O_2 gas bubbles produced on the cathode and anode, respectively, were insulating in nature [58]. Thus, the internal resistance of the cell [30] also increased from 2.28 to 4.42 Ω as I_{app} increased from 40 to 800 mA (Fig. 3b). Elsewhere, the measured E_A has a fundamental impact on the presence of radical species, as presented in the next section.

3.3. Validity of carbonate reactivity under advanced electrooxidation

The possible parallel reactions of sulfates and carbonates have also been investigated. A synthetic solution containing only HCO_3^-/CO_3^{2-} at 5 mmol L^{-1} (60 mg-C L^{-1}) and SO_4^{2-} at 5 mmol L^{-1} was studied at 40, 200 and 800 mA (Fig. 4). The evolution of sulfate concentration remained constant regardless of the applied current (Fig. 4a). This demonstrates the lack of reactivity of sulfates during electrolysis over this range of current densities with an interelectrode gap of 500 μm, while stronger operating conditions are known to form the sulfate radical at BDD anode surfaces [59]. In contrast, the evolution of TIC (i.e., carbonates) differed according to the applied current, see Fig. 4b. The carbonate concentration remained constant throughout electrolysis at 40 and 200 mA. However, at a higher current (800 mA), their concentration decreased exponentially with time ($R^2 = 0.91$) (Fig. 4c). At this intensity, E_A is around 3.0 V/Normal hydrogen electrode (NHE) (Fig. 3b). This is sufficient to generate physically sorbed $^{\bullet}OH$ at the BDD anode surface from H_2O oxidation (Eq. (13)), given its high O_2 evolution overvoltage (2.2–2.8 V/NHE) as well as the standard potential of the $^{\bullet}OH/H_2O$ redox couple, which is equal to 2.8 V/NHE [4–7]:

$$BDD + H_2O \rightarrow BDD(^{\bullet}OH) + e^- + H^+ \quad (13)$$

$^{\bullet}OH$ radicals are known to react with HCO_3^- and CO_3^{2-} to form carbonate radicals ($CO_3^{\bullet -}$), via a pseudo first-order reaction assuming a quasi steady-state approximation toward $^{\bullet}OH$ [50,51,60]. Thus, none of the carbonates was available to react with Ca^{2+} when the local pH was sufficiently high. This result could explain the lower $\Delta[Ca^{2+}]/\Delta[TIC]$ molar ratio at 800 mA, as shown in Fig. 2b. Additionally, the micro-distance (500 μm) used in the cell could favor the transport of carbonates towards the $^{\bullet}OH$ present in the vicinity of the anode surface, because such a small distance enhances mass transfer, as reported previously with a cell of the same design [21,29].

This result also highlighted the unprecedented anodic contribution to the limitation of cathodic $CaCO_3$ electroprecipitation at the current density leading to the formation of $^{\bullet}OH$. The contribution of radicals has been considered in a new mathematical model described in the following section and in the Supplementary Information.

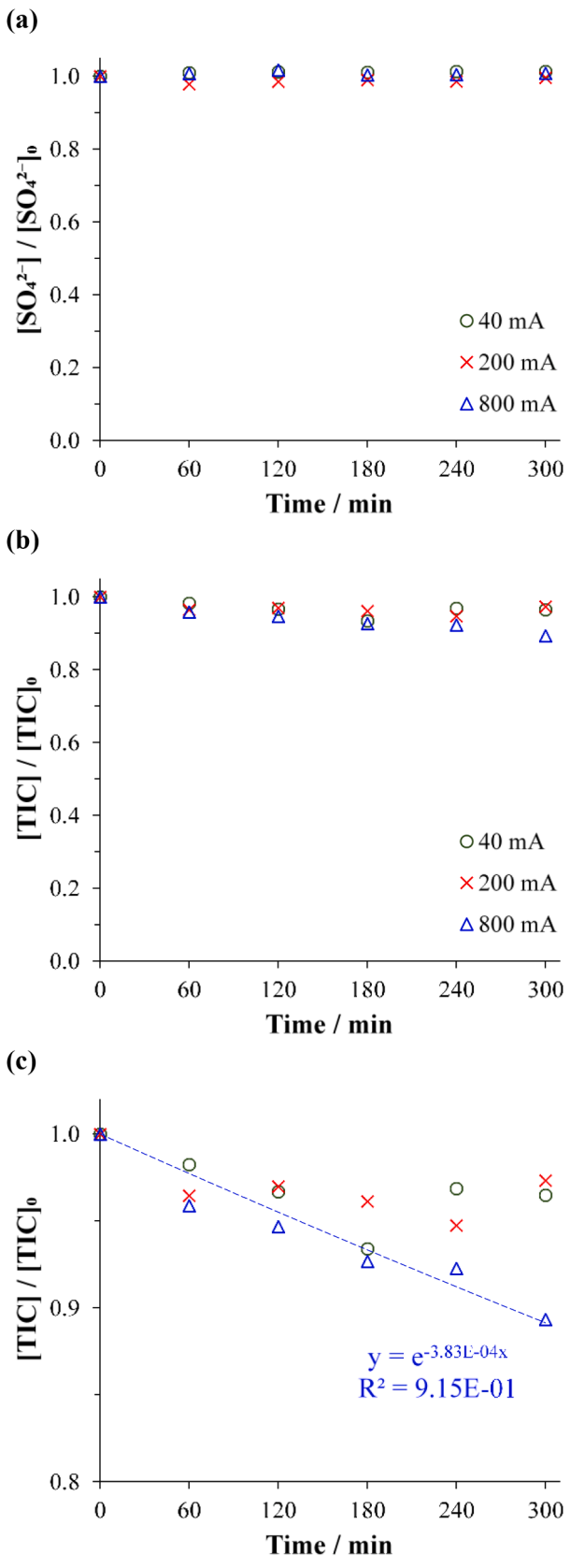

Fig. 4. Variation of (a) SO_4^{2-} and ((b), (c)) TIC in blank solution containing only HCO_3^-/CO_3^{2-} (5 mmol L^{-1}; 60 mg-C L^{-1}) and SO_4^{2-} (5 mmol L^{-1}) during electro-oxidation at 40, 200 and 800 mA.

3.4. Kinetics modeling and mechanistic scheme of $CaCO_3$ electroprecipitation

Considering the results presented in the previous sections, a novel kinetic model was developed for $CaCO_3$ electroprecipitation in a microfluidic thin film reactor under different current intensity conditions. This model is described in detail in the Methods section, the associated curves are plotted in Fig. 2 against experimental data, and Table S2 shows the primary constants involved in the model. Table S3 summarizes the data (initial conditions, variables and processes) computed using the Aquasim® software assuming a mixed reactor compartment type as well as a constant volume (5×10^{-4} m^3) with zero input (batch system). The difference in the kinetics of electroprecipitation depending on the applied current was modeled by considering **(i)** the gas hindrance factor (α) [30]; **(ii)** scale detachment (k_{det}) at the cathode due to high H_2 gas evolution at sufficiently low E_C values (200 and 800 mA conditions) [30]; and **(iii)** carbonate reactions with $^{\bullet}OH$ ($k_{\bullet OH}$) at higher currents (800 mA) when E_A was sufficiently high to produce $^{\bullet}OH$ (newly introduced in this study). $k_{\bullet OH}$ was determined experimentally by considering the slope in Fig. 4c (i.e., 3.83×10^{-4} min^{-1}).

RMSE values indicated good fits, particularly with the kinetics of Ca^{2+} concentration (RMSE < 0.19), while RMSE values were below 0.42 for TIC evolution. These results confirmed the critical role of current density in scale detachment and carbonate reactivity. A mechanistic scheme illustrating the different factors that affect $CaCO_3$ electroprecipitation is shown in Fig. S2.

4. Conclusions

The present work was stimulated by an interest in developing microreactors that not only allow electrical energy consumption to be minimized, but also operate with low-salinity effluents while decreasing electroprecipitation phenomena at a sufficiently high current density. The results demonstrate the possibility of limiting the frequency of polarity reversal at an industrial scale, though the anodic role (accumulation of $^{\bullet}OH$ and H^+) could be minimized depending on the operating conditions and the characteristics of the solution being treated. Moreover, this study highlights an additional feature to consider: the kinetics of $^{\bullet}OH$ reactivity in the degradation of organic pollutants during advanced electro-oxidation treatment in the presence of hard water.

There is still a need to carry out studies in presence of more complex matrices, whilst the generation of unwanted byproducts under various applied currents should be monitored and controlled. Other radical scavengers (nitrate, organic matter, etc.) could be in competition with carbonates and therefore limit the anti-scaling role of $^{\bullet}OH$. Moreover, the lower treatment capacity and higher clogging issues of microreactors encourages researchers to consider innovative designs [25,27,61]. A reactive electro-mixing reactor that combines both micro- and macro-reactors could be one possibility [25,27,61]. Finally, further studies are required to compare the cost efficiency of the anti-scaling effect demonstrated in this paper with other conventional descaling technologies (e.g. mechanical techniques).

CRediT authorship contribution statement

Faidzul Hakim Adnan: Methodology, Investigation, Software, Formal analysis, Writing – original draft. **Steve Pontvianne:** Investigation. **Marie-Noëlle Pons:** Supervision, Writing – review & editing, Funding acquisition. **Emmanuel Mousset:** Conceptualization, Methodology, Software, Validation, Supervision, Writing – original draft, Writing – review & editing, Project administration, Resources, Funding acquisition.

Declaration of Competing Interest

The authors declare that they have no known competing financial interests or personal relationships that could have appeared to influence the work reported in this paper.

Data availability

Data will be made available on request.

Acknowledgments

The authors would like to thank the French Ministry of Higher Education, Research and Innovation (MESRI) for financial support of Faidzul Hakim Adnan's doctoral program. They are also grateful for financial support provided by Carnot ICEEL, LTSER Zone Atelier du Bassin de la Moselle (ZAM) and the European regional development fund program (CPER SusChemProc).

Appendix A. Supplementary data

Supplementary data to this article can be found online at https://doi.org/10.1016/j.elecom.2023.107493.

References

[1] S.D. Richardson, S.Y. Kimura, Water analysis: emerging contaminants and current issues, Anal. Chem. 88 (2016) 546–582, https://doi.org/10.1021/acs.analchem.5b04493.
[2] M. Gros, M. Petrović, D. Barceló, Development of a multi-residue analytical methodology based on liquid chromatography-tandem mass spectrometry (LC-MS/MS) for screening and trace level determination of pharmaceuticals in surface and wastewaters, Talanta 70 (2006) 678–690, https://doi.org/10.1016/j.talanta.2006.05.024.
[3] O. Garcia-Rodriguez, E. Mousset, H. Olvera-Vargas, O. Lefebvre, Electrochemical treatment of highly concentrated wastewater: A review of experimental and modeling approaches from lab- to full-scale, Crit. Rev. Environ. Sci. Technol. 52 (2022) 240–309, https://doi.org/10.1080/10643389.2020.1820428.
[4] M.A. Oturan, J.-J. Aaron, Advanced oxidation processes in water/wastewater treatment: principles and applications. A review, Crit. Rev. Environ. Sci. Technol. 44 (2014) 2577–2641, https://doi.org/10.1080/10643389.2013.829765.
[5] I. Sirés, E. Brillas, Remediation of water pollution caused by pharmaceutical residues based on electrochemical separation and degradation technologies: a review, Environ. Int. 40 (2012) 212–229, https://doi.org/10.1016/j.envint.2011.07.012.
[6] C.A. Martínez-Huitle, M. Panizza, Electrochemical oxidation of organic pollutants for wastewater treatment, Curr. Opin. Electrochem. 11 (2018) 62–71, https://doi.org/10.1016/j.coelec.2018.07.010.
[7] P.V. Nidheesh, S.O. Ganiyu, C.A. Martínez-Huitle, E. Mousset, H. Olvera-Vargas, C. Trellu, M. Zhou, M.A. Oturan, Recent advances in electro-Fenton process and its emerging applications, Crit. Rev. Environ. Sci. Technol. 53 (8) (2023) 887–913.
[8] K. Groenen Serrano, in: Electrochemical Water and Wastewater Treatment, Elsevier, 2018, pp. 133–164.
[9] C. Sáez, M.A. Rodrigo, A.S. Fajardo, C.A. Martínez-Huitle, in: Electrochemical Water and Wastewater Treatment, Elsevier, 2018, pp. 165–192.
[10] J. Wang, R. Zhuan, Degradation of antibiotics by advanced oxidation processes: An overview, Sci. Total Environ. 701 (2020), 135023, https://doi.org/10.1016/J.SCITOTENV.2019.135023.
[11] E. Brillas, I. Sirés, in: Electrochemical Water and Wastewater Treatment, Elsevier, 2018, pp. 267–304.
[12] F.C. Moreira, R.A.R. Boaventura, E. Brillas, V.J.P. Vilar, Electrochemical advanced oxidation processes: A review on their application to synthetic and real wastewaters, Appl. Catal. B Environ. 202 (2017) 217–261, https://doi.org/10.1016/j.apcatb.2016.08.037.
[13] E. Mousset, W.H. Loh, W.S. Lim, L. Jarry, Z. Wang, O. Lefebvre, Cost comparison of advanced oxidation processes for wastewater treatment using accumulated oxygen-equivalent criteria, Water Res. 200 (2021), 117234, https://doi.org/10.1016/j.electacta.2021.138466.
[14] B.P. Chaplin, Critical review of electrochemical advanced oxidation processes for water treatment applications, Environ. Sci. Process. Impacts 16 (2014) 1182–1203, https://doi.org/10.1039/C3EM00679D.
[15] P. Rychen, C. Provent, L. Pupunat, N. Hermant, in: Domestic and industrial water disinfection using boron-doped diamond electrodes, in Electrochemistry for the Environment, Springer-Verlag, New York, 2010, pp. 143–161, https://doi.org/10.1007/978-0-387-68318-8_6/COVER.
[16] A. Kapalka, L. Joss, Á. Anglada, C. Comninellis, K.M. Udert, Direct and mediated electrochemical oxidation of ammonia on boron-doped diamond electrode, Electrochemistry Communications 12 (2010) 1714–1717, https://doi.org/10.1016/j.elecom.2010.10.004.
[17] C.A. Martínez-Huitle, E. Brillas, A critical review over the electrochemical disinfection of bacteria in synthetic and real wastewaters using a boron-doped diamond anode, Curr. Opin. Solid State Mater. Sci. 25 (4) (2021) 100926.
[18] E. Mousset, C. Trellu, H. Olvera-Vargas, Y. Pechaud, F. Fourcade, M.A. Oturan, Electrochemical technologies coupled with biological treatments, Curr. Opin. Electrochem. 26 (2021), 100668, https://doi.org/10.1016/j.coelec.2020.100668.
[19] C.A. Martínez-Huitle, M.A. Rodrigo, I. Sirés, O. Scialdone, Single and coupled electrochemical processes and reactors for the abatement of organic water pollutants: A critical review, Chem. Rev. 115 (2015) 13362–13407, https://doi.org/10.1021/acs.chemrev.5b00361.
[20] I. Sirés, E. Brillas, M.A. Oturan, M.A. Rodrigo, M. Panizza, Electrochemical advanced oxidation processes: today and tomorrow. A review, Environ. Sci. Pollut. Res. 21 (2014) 8336–8367, https://doi.org/10.1007/s11356-014-2783-1.
[21] J.F. Pérez, J. Llanos, C. Sáez, C. López, P. Cañizares, M.A. Rodrigo, Development of an innovative approach for low-impact wastewater treatment: A microfluidic flow-through electrochemical reactor, Chem. Eng. J. 351 (2018) 766–772, https://doi.org/10.1016/j.cej.2018.06.150.
[22] J.F. Pérez, J. Llanos, C. Sáez, C. López, P. Cañizares, M.A. Rodrigo, Towards the scale up of a pressurized-jet microfluidic flow-through reactor for cost-effective electro-generation of H2O2, J. Clean. Prod. 211 (2019) 1259–1267, https://doi.org/10.1016/j.jclepro.2018.11.225.
[23] O. Scialdone, A. Galia, S. Randazzo, Electrochemical treatment of aqueous solutions containing one or many organic pollutants at boron doped diamond anodes. Theoretical modeling and experimental data, Chem. Eng. J. 183 (2012) 124–134, https://doi.org/10.1016/j.cej.2011.12.042.
[24] O. Scialdone, A. Galia, S. Sabatino, Electro-generation of H2O2 and abatement of organic pollutant in water by an electro-Fenton process in a microfluidic reactor, Electrochem. Commun. 26 (2013) 45–47, https://doi.org/10.1016/j.elecom.2012.10.006.
[25] S. Ben Kacem, D. Clematis, S.C. Elaoud, A. Barbucci, M. Panizza, A flexible electrochemical cell setup for pollutant oxidation in a wide electrical conductivity range and its integration with ultrasound, J. Water Process Eng. 46 (2022), 102564, https://doi.org/10.1016/j.jwpe.2022.102564.
[26] E. Mousset, M. Puce, M.-N. Pons, Advanced electro-oxidation with boron-doped diamond for acetaminophen removal from real wastewater in a microfluidic reactor – Kinetics and mass transfer studies, ChemElectroChem 6 (2019) 2908–2916, https://doi.org/10.1002/celc.201900182.
[27] E. Mousset, Unprecedented reactive electro-mixing reactor: Towards synergy between micro- and macro-reactors? Electrochem. Commun. 118 (2020), 106787 https://doi.org/10.1016/j.elecom.2020.106787.
[28] F.H. Adnan, M.-N. Pons, E. Mousset, Thin film microfluidic reactors in electrochemical advanced oxidation processes for wastewater treatment: A review on influencing parameters, scaling issues and engineering considerations, Electrochem. Sci. Adv. (2022) e2100210.
[29] F.H. Adnan, M.-N. Pons, E. Mousset, Mass transport evolution in microfluidic thin film electrochemical reactors: New correlations from millimetric to submillimetric interelectrode distances, Electrochem. Commun. 130 (2021), 107097, https://doi.org/10.1016/j.elecom.2021.107097.
[30] F.H. Adnan, S. Pontvianne, M.N. Pons, E. Mousset, Unprecedented roles of submillimetric interelectrode distances and electrogenerated gas bubbles on mineral cathodic electro-precipitation: Modeling and interface studies, Chem. Eng. J. 431 (2022), 133413, https://doi.org/10.1016/j.cej.2021.133413.
[31] E. Mousset, Interest of micro-reactors for the implementation of advanced electrocatalytic oxidation with boron-doped diamond anode for wastewater treatment, Curr. Opin. Electrochem. 32 (2022), 100897, https://doi.org/10.1016/j.coelec.2021.100897.
[32] J.F. Pérez, J. Llanos, C. Sáez, C. López, P. Cañizares, M.A. Rodrigo, A microfluidic flow-through electrochemical reactor for wastewater treatment: A proof-of-concept, Electrochem. Commun. 82 (2017) 85–88, https://doi.org/10.1016/j.elecom.2017.07.026.
[33] P. Ma, H. Ma, S. Sabatino, A. Galia, O. Scialdone, Electrochemical treatment of real wastewater. Part 1: Effluents with low conductivity, Chem. Eng. J. 336 (2018) 133–140, https://doi.org/10.1016/j.cej.2017.11.046.
[34] F.H. Adnan, E. Mousset, S. Pontvianne, M.N. Pons, Mineral cathodic electro-precipitation and its kinetic modelling in thin-film microfluidic reactor during advanced electro-oxidation process, Electrochim. Acta 387 (2021), 138487, https://doi.org/10.1016/j.electacta.2021.138487.
[35] C. Deslouis, I. Frateur, G. Maurin, B. Tribollet, Interfacial pH measurement during the reduction of dissolved oxygen in a submerged impinging jet cell, J. Appl. Electrochem. 27 (1997) 482–492, https://doi.org/10.1023/A:1018430224622.
[36] M.M. Tlili, M. Benamor, C. Gabrielli, H. Perrot, B. Tribollet, Influence of the interfacial pH on electrochemical $CaCO_3$ precipitation, J. Electrochem. Soc. 150 (2003) C765, https://doi.org/10.1149/1.1613294/XML.
[37] Y. Ben Amor, L. Bousselmi, M.-C. Bernard, B. Tribollet, Nucleation-growth process of calcium carbonate electrodeposition in artificial water - Influence of the sulfate ions, J. Cryst. Growth 320 320 (1) (2011) 69–77.
[38] J.N. Butler, Carbon Dioxide Equilibria and Their Applications, CRC Press, New York, NY, 1991.
[39] K.J. Powell, P.L. Brown, R.H. Byrne, T. Gajda, G. Hefter, S. Sjöberg, H. Wanner, Chemical speciation of environmentally significant heavy metals with inorganic ligands. Part 1: The Hg^{2+} – Cl^-, OH^-, CO_3^{2-}, SO_4^{2-}, and PO_4^{3-} aqueous systems (IUPAC Technical Report), Pure Appl. Chem. 79 (2000) 895–950, https://doi.org/10.1351/PAC200779050895.

[40] C. Zhang, J. Tang, G. Zhao, Y. Tang, J. Li, F. Li, Investigation on an electrochemical pilot equipment for water softening with an automatic descaling system : Parameter optimization and energy consumption analysis, J. Clean. Prod. 276 (2020), 123178, https://doi.org/10.1016/j.jclepro.2020.123178.
[41] F.H. Adnan, S. Pontvianne, M.-N. Pons, E. Mousset, Roles of H_2 evolution overpotential, materials porosity and cathode potential on mineral electro-precipitation in microfluidic reactor – New criterion to predict and assess interdependency, Electrochim. Acta 428 (2022), 140926, https://doi.org/10.1016/j.electacta.2022.140926.
[42] L.F. Arenas, C. Ponce de León, F.C. Walsh, 3D-printed porous electrodes for advanced electrochemical flow reactors: A Ni/stainless steel electrode and its mass transport characteristics, Electrochem. Commun. 77 (2017) 133–137, https://doi.org/10.1016/j.elecom.2017.03.009.
[43] I. Sanjuán, D. Benavente, V. García-García, E. Expósito, V. Montiel, Electrochemical softening of concentrates from an electrodialysis brackish water desalination plant: Efficiency enhancement using a three-dimensional cathode, Sep. Purif. Technol. 208 (2019) 217–226, https://doi.org/10.1016/J.SEPPUR.2018.01.066.
[44] Y. Yu, H. Jin, X. Quan, B. Hong, X. Chen, Continuous multistage electrochemical precipitation reactor for water softening, Ind. Eng. Chem. Res. 58 (2019) 461–468, https://doi.org/10.1021/ACS.IECR.8B04200/SUPPL_FILE/IE8B04200_SI_001.PDF.
[45] K.H. Yeon, J.H. Song, J. Shim, S.H. Moon, Y.U. Jeong, H.Y. Joo, Integrating electrochemical processes with electrodialysis reversal and electro-oxidation to minimize COD and T-N at wastewater treatment facilities of power plants, Desalination 202 (2007) 400–410, https://doi.org/10.1016/J.DESAL.2005.12.080.
[46] F. Valero, R. Arbós, Desalination of brackish river water using electrodialysis reversal (EDR). Control of the THMs formation in the Barcelona (NE Spain) area, Desalination 253 253 (1-3) (2010) 170–174.
[47] H. Jin, Y. Yu, L. Zhang, R. Yan, X. Chen, Polarity reversal electrochemical process for water softening, Sep. Purif. Technol. 210 (2019) 943–949, https://doi.org/10.1016/J.SEPPUR.2018.09.009.
[48] Y. Yu, H. Jin, X. Jin, R. Yan, L. Zhang, X. Chen, Current pulsated electrochemical precipitation for water softening, Ind. Eng. Chem. Res. 57 (2018) 6585–6593, https://doi.org/10.1021/ACS.IECR.8B00448/ASSET/IMAGES/MEDIUM/IE-2018-00448R_0013.GIF.
[49] A. Lissaneddine, M.-N. Pons, F. Aziz, N. Ouazzani, L. Mandi, E. Mousset, A critical review on the electrosorption of organic compounds in aqueous effluent – Influencing factors and engineering considerations, Environ. Res. 204 (2022), 112128.
[50] J.M. Barazesh, C. Prasse, D.L. Sedlak, Electrochemical transformation of trace organic contaminants in the presence of halide and carbonate ions, Environ. Sci. Technol. 50 (2016) 10143–10152, https://doi.org/10.1021/ACS.EST.6B02232/ASSET/IMAGES/LARGE/ES-2016-02232F_0007.JPEG.
[51] A. Irkham, G. Fiorani, N. Valenti, F. Kamoshida, Y. Paolucci, Einaga, Electrogenerated chemiluminescence by in situ production of coreactant hydrogen peroxide in carbonate aqueous solution at a boron-doped diamond electrode, J. Am. Chem. Soc. 142 (2020) 1518–1525, https://doi.org/10.1021/JACS.9B11842/SUPPL_FILE/JA9B11842_SI_001.PDF.
[52] F. Sopaj, N. Oturan, J. Pinson, F.I. Podvorica, M.A. Oturan, Effect of cathode material on electro-Fenton process efficiency for electrocatalytic mineralization of the antibiotic sulfamethazine, Chem. Eng. J. 384 (2020), 123249, https://doi.org/10.1016/j.cej.2019.123249.
[53] P. Reichert, AQUASIM 2.0 – User manual: Computer program for the identification and simulation of aquatic systems, Swiss Federal Institute for Environmental Science and Technology (EAWAG), Dübendorf (1998).
[54] E. Mousset, L. Frunzo, G. Esposito, E.D. van Hullebusch, N. Oturan, M.A. Oturan, A complete phenol oxidation pathway obtained during electro-Fenton treatment and validated by a kinetic model study, Appl. Catal. B Environ. 180 (2016) 189–198, https://doi.org/10.1016/j.apcatb.2015.06.014.
[55] J. Marín-Cruz, R. Cabrera-Sierra, M.A. Pech-Canul, I. González, Characterization of different allotropic forms of calcium carbonate scales on carbon steel by electrochemical impedance spectroscopy, J. Appl. Electrochem. 34 (2004) 337–343, https://doi.org/10.1023/B:JACH.0000015648.68779.c6.
[56] S.M. Hoseinieh, T. Shahrabi, B. Ramezanzadeh, M.F. Rad, The role of porosity and surface morphology of calcium carbonate deposits on the corrosion behavior of unprotected API 5L X52 rotating disk electrodes in artificial seawater, J. Electrochem. Soc. 163 (2016) C515–C529, https://doi.org/10.1149/2.0191609jes.
[57] M. Ciobanu, J.P. Wilburn, M.L. Krim, D.E. Cliffel, in Handbook of Electrochemistry (C Zoski, Ed.), Elsevier, 2007.
[58] R. Hreiz, L. Abdelouahed, D. Fünfschilling, F. Lapicque, Electrogenerated bubbles induced convection in narrow vertical cells: PIV measurements and Euler-Lagrange CFD simulation, Chem. Eng. Sci. 134 (2015) 138–152, https://doi.org/10.1016/j.ces.2015.04.041.
[59] J. Davis, J.C. Baygents, J. Farrell, Understanding persulfate production at boron doped diamond film anodes, Electrochim. Acta 150 (2014) 68–74, https://doi.org/10.1016/j.electacta.2014.10.104.
[60] B.P. Chaplin, Advantages, disadvantages, and future challenges of the use of electrochemical technologies for water and wastewater treatment, In Electrochemical Water and Wastewater Treatment (2018) 451–494, https://doi.org/10.1016/B978-0-12-813160-2.00017-1.
[61] E. Mousset, T.A. Hatton, Advanced hybrid electro-separation/electro-conversion systems for wastewater treatment, reuse and recovery: compromise between symmetric and asymmetric constraints, Curr. Opin. Electrochem. 35 (2022), 101105, https://doi.org/10.1016/j.coelec.2022.101105.